ELSEVIER

Journal of Alloys and Compounds 455 (2008) 413–419

Journal of ALLOYS AND COMPOUNDS

www.elsevier.com/locate/jallcom

# Investigation of ballistic impact properties and fracture mechanisms of $Ti_3SiC_2$ ternary ceramics

Wen-Tse Lo [a], Ching-An Jeng [b], Jow-Lay Huang [a,*], Horng-Hwa Lu [c], Ding-Fwu Lii [d]

[a] *Department of Materials Science and Engineering, National Cheng Kung University, No. 1, University Road, Tainan City 70101, Taiwan, ROC*
[b] *Department of Mechanical and Automation Engineering, I-Shou University, Kaohsiung County 84001, Taiwan, ROC*
[c] *Department of Mechanical Engineering, National Chin-Yi Institute of Technology, Taichung County 41101, Taiwan, ROC*
[d] *Department of Electrical Engineering, Cheng Shiu University, Kaohsiung County 83347, Taiwan, ROC*

Received 29 December 2006; received in revised form 23 January 2007; accepted 23 January 2007
Available online 28 January 2007

**Abstract**

The deformation response of $Ti_3SiC_2$ ternary ceramics have been investigated by performing ballistic impact experiments at a range of low velocities. The reactively hot pressing compacts with an off-stoichiometric ratio were predominantly $Ti_3SiC_2$ phase (99.13 vol.%) and the grains were elongated in shape with a grain size of 3–8 μm. The bulk modulus (196 GPa) was slightly lower than that calculated by fitting the pressure versus lattice volume data with the Birch–Murnaghan equation (206 GPa), and that predicted by using the first-principle computational technique (204 GPa). The typical fracture surface of the fragments was failed by transgranular fracture combined with intergranular fracture. Most fracture mechanisms were similar to energy-absorbing mechanisms observed in the vicinity of the indentation. The dynamically impacted fragments of $Ti_3SiC_2$ contained dislocations and stacking faults, grouped in bands extending from the grain boundaries and ending in the grain. The Si plane was depleted and the remaining thin lamella consisted of six close-packed Ti planes, with five C planes in-between, showing identical stacking as {1 1 1} planes in TiC. The Hugoniot elastic limit and the hydronamic pressure at the HEL point were estimated to be 6 and 3 GPa, respectively.


*Keywords:* $Ti_3SiC_2$ ternary ceramics; Ballistic impact; Fracture mechanisms; Microstructure; Mechanical properties

## 1. Introduction

Titanium silicon carbide ($Ti_3SiC_2$) is the first MAX phase material (where M is an early transition metal, A is an A-group element, mostly IIIA and IVA, and X is either C or N) with an unusual combination of electrical, thermal, and mechanical properties [1–4]. The unique properties may be attributed to its hexagonal structure with planar Si layers linked together by TiC octahedrons, forming a deformable basal slip plane. It has excellent machinability and it is not susceptible to thermal shock up to 1400 °C for a coarse grain [5], and can be considered for a number of structural applications like engine parts. The low ratio of hardness/Young's modulus suggests that the mechanical behavior is similar to that of ductile metals due to its partial metallic bonding and the presence of mobile basal plane dislocations [6].

More recently, it has been shown that MAX phase materials belong to kinking nonlinear elastic solids that includes graphite, layered silicates, and ice, because kinking plays a key role in their deformation [7]. Under compression, many of the MAX phase materials deform plastically by the formation of shear bands [6,8]. The shear bands have a high volume fraction of voids and cavities that are bridged by ligaments. Onodera et al. [9] measured the static high pressure compressibility with synchrotron X-ray diffraction. They found that the compressibility along the *a* direction is higher than that along the *c* direction. The incompressibility and the ductile metal-like deformation response of this ternary carbide ceramic make it a potentially damage tolerant material.

Despite the fact that these materials are elastically quite stiff and very stable up to pressures of at least about 50 GPa [5,9–10], they are relatively soft with Vickers hardness values between 2 and 5 GPa [5]. The dynamic responses of brittle materials to impact results are primarily from an interest in their possible use as armor materials or engine turbine blades. With hardnesses, they are relatively soft for ceramics but harder than most metals.

* Corresponding author. Tel.: +886 6 2348188; fax: +886 6 2763586.
*E-mail address:* jlh888@mail.ncku.edu.tw (J.-L. Huang).

0925-8388/$ – see front matter © 2007 Elsevier B.V. All rights reserved.
doi:10.1016/j.jallcom.2007.01.117

For defence and aeronautical applications, it is necessary to understand what happens to the material when it is subjected to impact.

The purpose of this study is to report on damage observed in hot-pressed $Ti_3SiC_2$ generated by a penetrating impact with a handgun bullet at a velocity of 380 m/s. The microstructure and fracture mechanisms of $Ti_3SiC_2$ ternary ceramics suffered ballistic impact are also investigated.

## 2. Experimental procedure

### 2.1. Samples preparation

The starting powders of Ti (Titanium, −325 mesh, 99.5% Alfa Aesar, Ward Hill, MA, USA), SiC (Silicon Carbide, −400 mesh, Aldrich, Milwaukee, Wisconsin, USA), C (Graphite, 1–2 μm, 99.99% Aldrich, Milwaukee, WI, USA) and Si (Silicon, −325 mesh, 99.999%, Cerac Inc., Milwaukee, WI, USA) were used to synthesize $Ti_3SiC_2$ bulk samples. Silicon-rich compositions with Ti:SiC:C:Si = 3:1:1:0.1 molar ratios were ball-milled for 24 h in ethanol using high-purity silicon nitride spherical media. The powders were dried, screened, and pressed into discs of 50 mm (diameter) × 10 mm (thickness) under a uniaxial pressure of 10 MPa prior to hot pressing at a mechanical pressure of 25 MPa inside graphite dies in 0.1 MPa Ar atmosphere at a temperature of 1500 °C for 1 h.

### 2.2. Phase and microstructural analysis

The phase composition and microstructure of samples were analyzed by an X-ray diffractometer (XRD, D/Max-IIB, Rigaku Corporation, Tokyo, Japan). Samples were scanned from 20° to 80° with Cu Kα radiation and an Ni filter at 30 kV and 20 mA with a scanning rate of 4°/min. Field emission scanning electron microscopy (FE-SEM, XL40 FEG, Phillips, Eindhoven, The Netherlands) equipped with an energy dispersive X-ray spectrometer (EDX, DX-4, EDAX Inc., Mahwah, NJ, USA) was used to examine the microstructure and elementary analysis of hot-pressed samples. Samples for SEM analysis were cut, ground, and polished to 1 μm diamond suspension. Typical SEM micrographs were revealed by chemical etching with a solution of water, nitric acid, and hydrofluoric acid 2:1:1 by volume percent for 10 s. Thin foils for transmission electron microscopy (TEM) investigations were prepared by mechanically grinding the ceramic pellets to a thickness of 20–30 μm. The samples were mounted on copper aperture grids, and final thinning was conducted via argon-ion milling (Model 600 Dual Ion Mill, Gatan Inc., Pleasanton, CA, USA). Electron diffraction and high-resolution electron microscopy (HREM) were performed at 200 kV (FEG-TEM, Tecnai $G^2$ F20, Philips, Eindhoven, The Netherlands).

### 2.3. Mechanical properties

The hot-pressed billets were machined into bars with a dimension of 3 mm × 4 mm × 45 mm as specified by ASTM Standard (ASTM E855-81) and polished to 1 μm diamond suspension. Flexural strength was measured by a four-point bending test on a universal testing instrument (Series 8511, Instron Corporation, MA, USA) using a 40 mm support span and a 20 mm loading span, with the crosshead speed at 0.5 mm/min. Fracture toughness was measured using the Single Edge Notched Beam (SENB) method with a 0.02 mm (width) × 1 mm (length) crack. All crack planes were parallel to the hot-pressing direction. A Vikers hardness machine (Model AVK-C21, Akashi Co., Yokohama, Japan) was used to obtain hardness data at a load of 100 N. The elastic modulus and Poisson's ratio were evaluated by pulse echo method (Pulse Generator, Model 5072, Panametrics, Inc., Waltham, MA, USA; Oscilloscope, Model TDS540C, Tektronix, Inc., Beaverton, OR, USA).

### 2.4. Ballistic impact testing

The ballistic testing was conducted using a 9 mm × 19 mm Parabellum type cartridge (TC 95), with a bullet weight of 7.45 g, as projectiles. A $Ti_3SiC_2$ disc of 50 mm (diameter) × 4 mm (thickness) was attached to an Al fixture ring, equally spaced around the circumference by socket bolts. The target assemblies were inserted into a polywood box placed at a distance of 5 m from the gun exit and adjusted to ensure that the center of the target block corresponded with the center of the shot-line. Bullet velocity was measured using the normal sight-screen arrangement just before the target. The schema of ballistic impact experiment is shown in Fig. 1. After the impact, the target assemblies were removed from the mounting fixture and pieces of the ceramic were recovered. The pieces were sectioned, mounted, and polished for microstructural characterization.

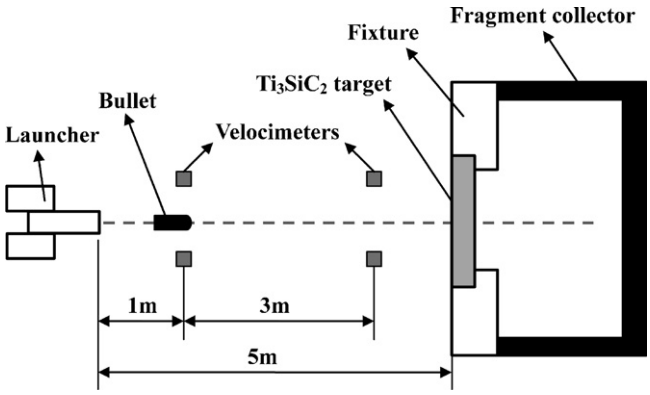


Fig. 1. The schema of ballistic impact experiment.

## 3. Results and discussions

### 3.1. Characterization of $Ti_3SiC_2$

Fig. 2 is a typical microstructure of $Ti_3SiC_2$ ceramic formed by hot pressing at 1500 °C under a mechanical pressure of 25 MPa for 1 h in 0.1 MPa Ar atmosphere. The $Ti_3SiC_2$ grains in reactively sintered compacts with an off-stoichiometric ratio are elongated in shape with a grain size of 3–8 μm. The small bright particles and acute blocks located among the $Ti_3SiC_2$ grains matrix, with little abnormal grain-growth behavior, are TiC phase. TiC phase has been proven to inhibit grain growth from the reaction path and microstructure evolution by a reactive hot isostatic pressing technique [3]. A summary of the $Ti_3SiC_2$ content, as well as the physical, mechanical, and acoustic properties of the hot-pressed specimen are listed in Table 1. Based on X-ray diffraction patterns, the $Ti_3SiC_2$ content was calcu-

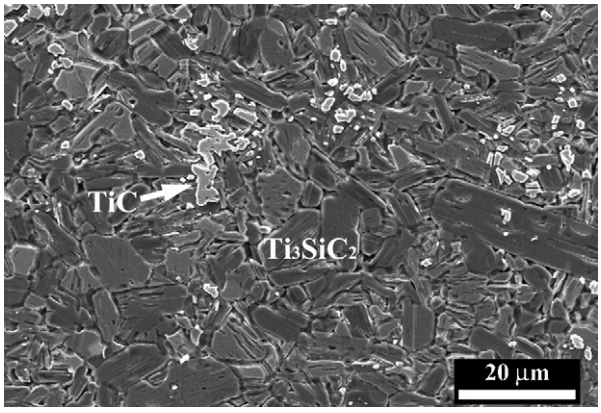


Fig. 2. SEM micrograph of hot-pressed and etched $Ti_3SiC_2$.

Table 1
Characteristic of physical, mechanical, and acoustic properties of $Ti_3SiC_2$ specimen hot-pressed with 3Ti/SiC/C/0.1Si mixtures at 1500 °C under a pressure of 25 MPa in 0.1 MPa Ar for 1 h.

| Property | Value |
|---|---|
| $Ti_3SiC_2$ content (vol.%) | 99.13 |
| Apparent density (g/cm$^3$) | 4.51 |
| 4-p bending strength (MPa) | $335 \pm 20$ |
| Fracture toughness (MPa m$^{1/2}$) | $7 \pm 0.3$ |
| Vickers hardness (GPa) | $3 \pm 0.3$ |
| Longitudinal wave speed (km/s) | 9.35 |
| Shear wave speed (km/s) | 5.69 |
| Young's modulus (GPa) | $353 \pm 5.62$ |
| Shear modulus (GPa) | $147 \pm 3.75$ |
| Poisson's ratio | 0.2 |

lated using the calibrated standard addition method [11], with a result of 99.13 vol.%. The room-temperature bending strength and toughness of samples were 335 MPa and 7 MPa m$^{1/2}$, respectively. The high toughness value is quite respectable compared to layered compounds such as mica and graphite, due to their elongated and platelet shape structure [8]. The Vickers hardness of $Ti_3SiC_2$ is 3 GPa. In contrast to most ceramics, the indent exhibits a pileup of material and the absence of cracks emanating from indent corners. Obviously, this is more comparable to that of ductile metals than typical ceramics.

The bulk modulus represents the resistance to volume change and is related to the overall atomic binding properties of a material. The measured bulk modulus of the $Ti_3SiC_2$ sample used in this study, calculated from the Young's modulus (353 GPa) and Poisson's ratio (0.2) from Table 1, is 196 GPa, slightly lower than that calculated by fitting the pressure versus lattice volume data with the Birch–Murnaghan equation (206 GPa) [9,10], but about 10% higher than the values calculated from the longitudinal and transverse velocities of sound (179 GPa) [12]. The theoretical simulation value of the bulk modulus of $Ti_3SiC_2$ ceramics, predicted by using first-principle computational technique is 204 GPa [13], in agreement with the static pressure fitting value of 206 GPa [10]. Base on the previous calculations and comparison of bulk modulus of $Ti_3SiC_2$ ternary ceramics estimated from various methods, $Ti_3SiC_2$ shows an anomalous behavior [10]. It is very incompressible due to its similar bulk modulus (~206 GPa) to that of TiC (~220 GPa). Its elastic modulus (~320 GPa) and shear modulus (~133 GPa) are similar to those of metallic molybdenum (elastic modulus = 318 GPa and shear modulus = 122 GPa). On the other hand, its hardness is comparable to that of quenched high carbon steels. The unique properties of this ternary ceramic are attributed to its layered structure, which consists of TiC octahedrons separated by layers of silicon atoms. The incompressibility and the metal-like deformation response of this ternary ceramic make it a potentially interesting damage tolerant armor material.

### 3.2. Response of ballistic impact

The $Ti_3SiC_2$ sample was impacted using ballistic testing, and the larger fragments were rearranged as shown in Fig. 3(a). The

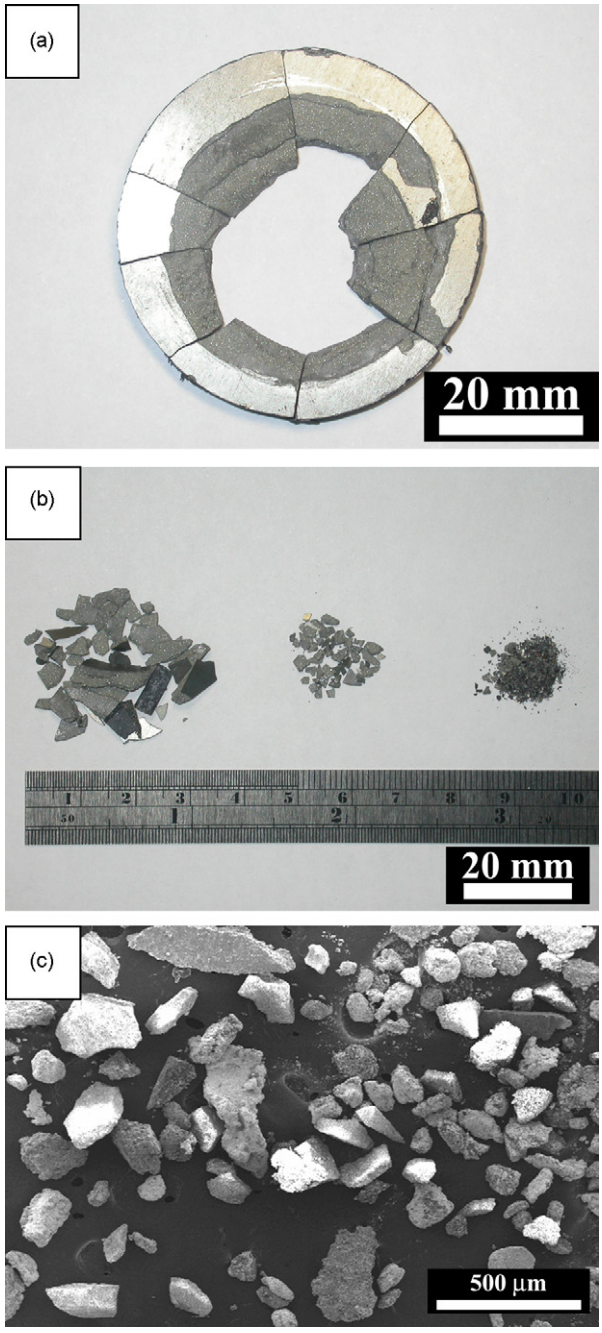


Fig. 3. (a and b) Optical micrographs of recovered fragments, and (c) SEM micrograph of fine particles.

highly damaged fine particles were separated into roughly three groups and the high-magnification micrograph of finest particles are shown in Fig. 3(b) and (c), respectively. The impacted sample was completely penetrated and fracture damage was heaviest in a region just beneath the impacted site. Cone cracks, tangential cracks, and eight dominant radial cracks were observed. Various types of cracks formed during the ballistic impact have been studied with ceramics bonded with different backing materials [14,15]. A locus of conoid coaxial cracks starts at the impact point. Radial tensile cracks initiate at the back surface close to the axis of impact as a result of bending induced by local defor-

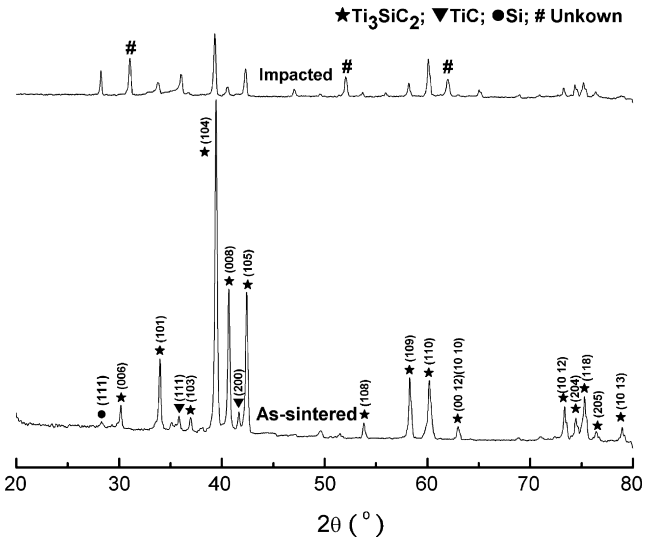


Fig. 4. X-ray diffraction patterns of an as-sintered $Ti_3SiC_2$ sample and the recovered powder after impact.

mation. Subsequently, a shear-dominated cone crack propagated from the edge of the contact zone.

Comminution and erosion occured at the cone area of the samples. The recovered fragments of damaged $Ti_3SiC_2$ had various sizes, ranging from chunks to a fine powder. Because the most platelike fragment shape did not vary with fragment size, it could be attributed to a particular layered structure of this compound.

Grady [16] proposed an analytical model, based on the balance between the kinetic energy and the newly created surface energy, to predict the fragment size:

$$d = \left( \frac{\sqrt{20} K_{IC}}{\rho c \dot{\varepsilon}} \right)^{2/3} \quad (1)$$

where $d$ is the fragment size, $K_{IC}$ the fracture toughness, $\rho$ the density, $c$ the sonic velocity, and $\dot{\varepsilon}$ is the strain rate. This equation shows that the fragment size increases with the material resistance to cracking ($K_{IC}$). From the average fragment size of about 2 mm shown in Fig. 3(b), an estimate of average strain rate is in a range of two orders of magnitude. Shih et al. [17] compared the dynamic deformation of SiC with a compression Hopkinson–Kolsky bar and high-velocity impact. They found that the predicted fragment size is about one order of magnitude larger than the measured fragment size. They proposed that plastic deformation and internal damage play a significant role in dynamic fragmentation.

A comparison between X-ray patterns of an as-sintered $Ti_3SiC_2$ sample with internal Si calibrated, and the recovered powder after impact is shown in Fig. 4. The results indicate that no phase transformation was observed, in spite of some unknown peaks corresponding to bullet contamination. Theoretical simulation predicts that the α- to β-$Ti_3SiC_2$ phase transformation results from the large shear strain [18]. From a previous study, the compression behavior of $Ti_3SiC_2$ does not exhibit the occurrence of the β-$Ti_3SiC_2$ phase upon compression up to 61 GPa [9]. It is clear that the impact pressure in the ballistic test is lower than the pressure of 49 GPa observed in the shock-loading conditions under plate impact experiment [10].

The strength of a material under plane shock wave loading can be defined in various ways. For example, it can be defined as the stress or strain at which a further increase in stress or strain causes the material to deform inelastically, i.e., its Hugoniot elastic limit (HEL); or it can be defined as the stress or strain where it loses cohesiveness under shock induced tension, i.e., its spall threshold; or it can be defined as the shear stress sustained by a material under shock compression above its HEL. Under plane shock wave loading, ceramics and metals in general show a distinctly different response with regard to their spall strengths under tensile wave loading. Whereas ceramics tend to have a lower value of tensile strength, i.e., a spall threshold lower in magnitude than the value of the compressive Hugoniot elastic limit, the spall threshold for metals tends to be higher than its HEL. Ceramics tend to have a large magnitude of HEL and a small magnitude of spall threshold, typically 5–10% of the value of their HEL. However, the shear stress sustained by metals and ceramics does not seem to reflect any such generally characterized difference. To explain the lower values of spall

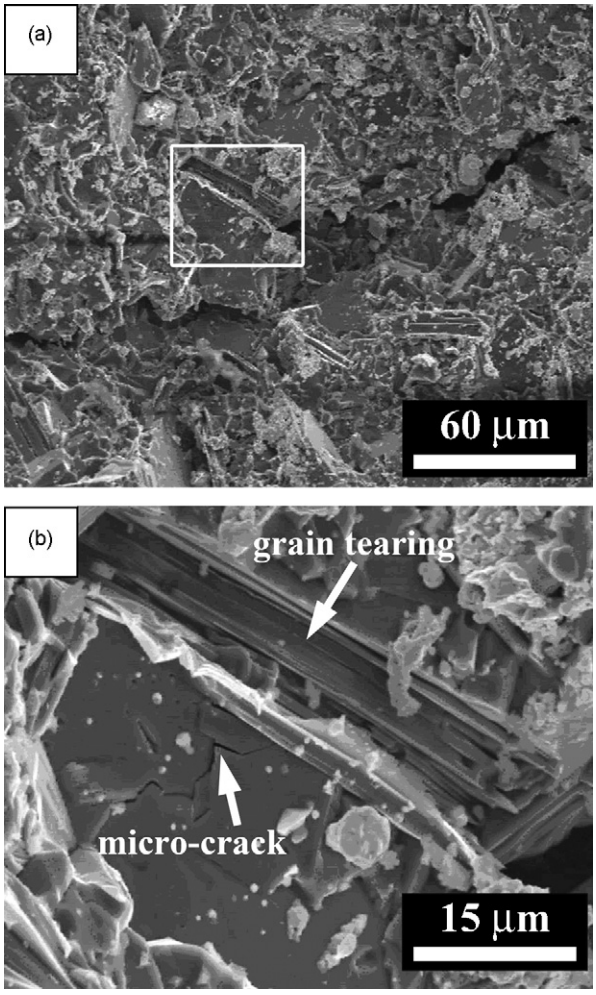


Fig. 5. (a) The typical fractured surface of recovery fragment of $Ti_3SiC_2$ after ballistic test. (b) Higher magnification of square area in (a) showing grain tearing and micro-cracks.

threshold in ceramics, it has been suggested that the generation of defects under shock compression causes ceramics to disintegrate under a smaller dynamic tensile stress loading compared to their compressive strengths (HEL).

The Hugoniot elastic limit ($\sigma_{HEL}$), a measure of the axial stress at which a solid is loaded under uniaxial compression, was estimated from the relationship derived by Rosenberg [19] from Griffith's yield criterion:

$$\sigma_{HEL} = \frac{1-\upsilon}{(1-2\upsilon)^2} Y \quad (2)$$

where $\nu$ is the Poisson's ratio and $Y$ is the equivalent dynamic compressive strength.

According to Griffith's biaxial stress yield criterion, $Y = 8\sigma_0$, where $\sigma_0$ is the tensile strength under uniaxial stress tension. In this study, using a tensile strength $\sigma_0$ of 335 MPa, and the Poisson's ratio $\nu$ of 0.2 for $Ti_3SiC_2$, we found that the Hugoniot elastic limit of this material is 6 GPa. The hydronamic pressure at the HEL point is calculated by the relationship:

$$p = \frac{K}{K + 4/3G} \times \sigma_{HEL} \quad (3)$$

where $K$ and $G$ are the bulk and shear moduli, respectively. The estimated hydronamic pressure is approximately 3 GPa. The strain rates involved in a plate experiment are higher ($10^4$ to $10^5\ s^{-1}$) than those which characterize uniaxial stress experiments ($10^2$ to $10^3\ s^{-1}$), like the Hopkinson experiment. In this intermediate rate regime, the failure stresses of $Al_2O_3$ and SiC increase slowly with strain rates up to $10^3\ s^{-1}$ [20]. It can be concluded that the interaction between cracks and the microstructure are slightly dependent of strain rate in the ballistic region.

### 3.3. Mechanisms of dynamic deformation

Fig. 5(a) is the typical fracture surface of the fragments, showing a feature of transgranular fracture combined with intergranular fracture. These fracture modes under impact deformation are similar to the fracture modes under a quasistatic indent. The high-magnification micrograph in Fig. 5(b) reveals the damage to consist predominantly of a tearing grain, with accompanying grain buckling, and micro-cracks. In order to compare the dynamic fracture mechanism with indentation loading experiments, the fracture surfaces of the cracked fragments were also examined. Various mechanisms of impact damage can be observed clearly in the SEM micrographs shown in Fig. 6. The laminate fracture, delamination, and grain pull-out were observed in fracture surfaces as shown in Fig. 6(a)–(c), respectively. A number of the delaminated grains were buckled into wavy shapes as shown in Fig. 6(d). Most mechanisms are similar to energy-absorbing mechanisms observed in the vicinity of the indentation [21].

Fig. 7 is a TEM micrograph of $Ti_3SiC_2$ specimens which suffered ballistic impact. The dynamically impacted fragments of $Ti_3SiC_2$ contained stacking faults and dislocations, as shown in Fig. 7(a). Stacking faults were grouped in bands extending from the grain boundaries and ending in the grain. Arrays of parallel dislocations are observed near some triple junctions and grain boundaries. This is consistent with observations by Farber et al. [22], who showed that both stacking faults and dislocations can easily be found in a reactive hot pressing sample of $Ti_3SiC_2$ during room temperature deformation. The stacking faults plane was identified as $\{0\,0\,0\,1\}$ in Fig. 7(b), and HRTEM images of a basal-plane stacking faults emanating from grain boundary

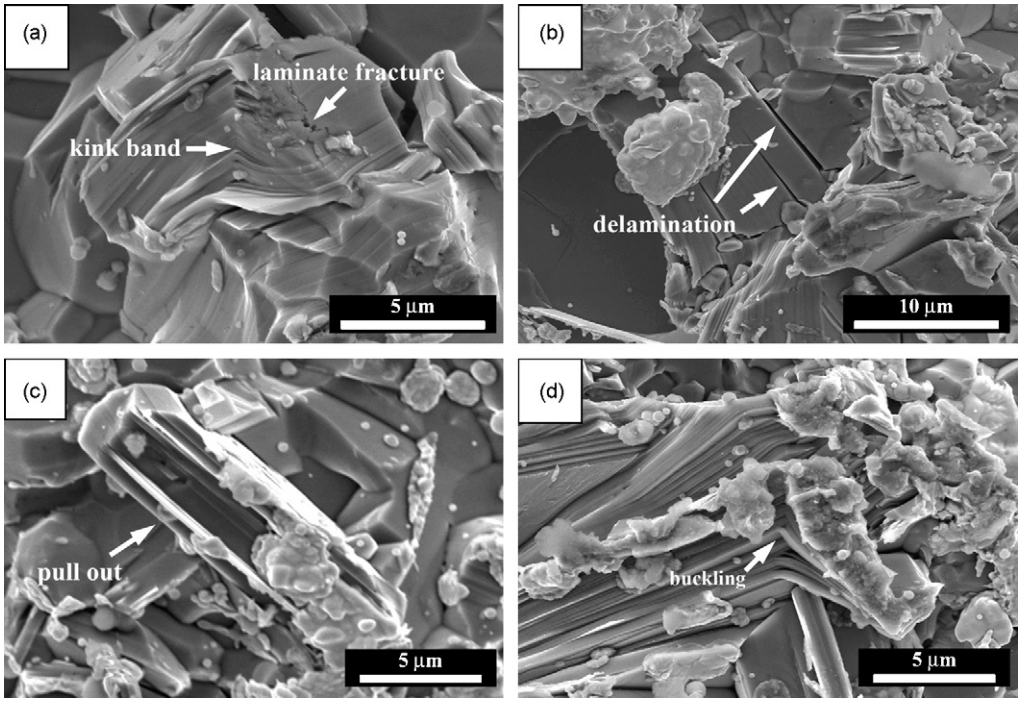


Fig. 6. Microstructural features associated with impact damage showing (a) laminate fracture and kink band, (b) delamination, (c) grain pull-out, and (d) grain buckling.

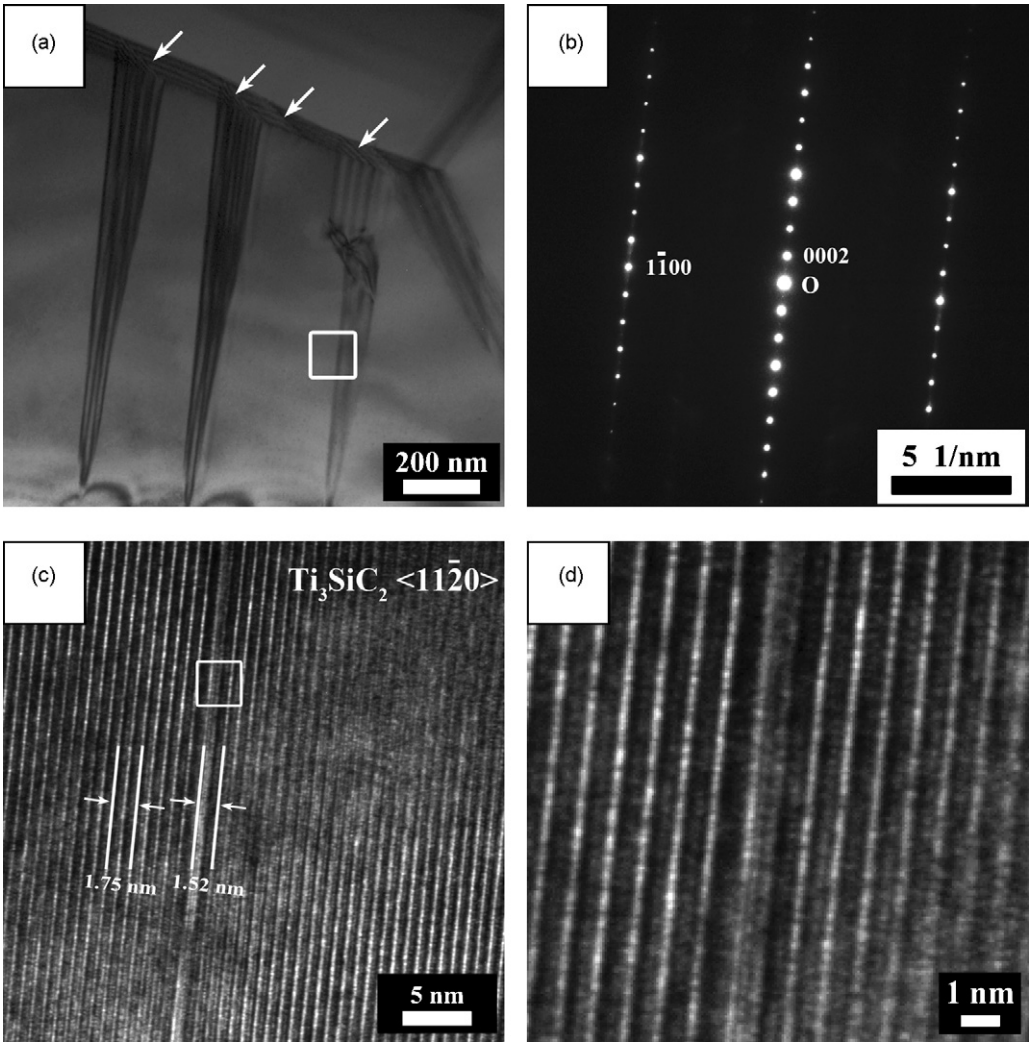


Fig. 7. (a) Stacking faults are grouped in bands extending from the grain boundary, and (b) related pattern. (c) HRTEM images of a basal plane stacking fault located at the square area shown in (a), and (d) Higher magnification of square area shown in (c).

are shown in Fig. 7(c) and (d). When the Si plane is depleted, stacking faults can be induced in $Ti_3SiC_2$. The remaining thin lamella consisted of six close-packed Ti planes and five C planes in-between, showing identical stacking as {1 1 1} planes of TiC. The formation of stacking faults has two models. Kooi et al. [23] had demonstrated that the local stresses generated by indentation can create the same stacking faults. Yu et al. [24] had reported that stacking faults result from insertion of additional TiC layers, instead of dissociation of dislocation. The latter could not originate from a simple shearing operation after impact deformation. The formation mechanism of stacking faults in the specimens which suffered ballistic impact in this study would be consistent with the former statement.

## 4. Conclusions

The ballistic penetrating impact experiments were first performed on $Ti_3SiC_2$ ceramics in this study. $Ti_3SiC_2$ samples were synthesized by reactive hot pressing of 3Ti/SiC/C/0.1Si powders mixture containing excess silicon at 1500 °C under a mechanical pressure of 25 MPa for 1 h in 0.1 MPa Ar atmosphere. The $Ti_3SiC_2$ content was calculated to be 99.13 vol.% and the elongated grains had a grain size of 3 to 8 μm. The bulk modulus, (196 GPa) was slightly lower than that calculated by fitting the pressure versus lattice volume data (206 GPa), and that predicted by using simulation (204 GPa). The typical fracture surface of the fragments exhibited transgranular fracture combined with intergranular fracture features. The laminate fracture, delamination, grain pull-out, and grain buckling appearances were observed in fracture surfaces. Stacking faults were grouped in bands extending from the grain boundaries and ending in the grain. The Si plane was depleted and the remaining thin lamella consist of six close-packed Ti planes, with five C planes in-between, showing identical stacking as {1 1 1} planes in TiC.

## Acknowledgments

The authors would like to thank the National Science Council, Republic of China, for its support under Grant No. NSC 94-2216-E-006-028.

## References


[1] M.W. Barsoum, T. El-Raghy, J. Am. Ceram. Soc. 79 (1996) 1953.
[2] C. Racault, F. Langlais, R. Naslain, J. Mater. Sci. 29 (1994) 3384.
[3] T. El-Raghy, M.W. Barsoum, J. Am. Ceram. Soc. 82 (1999) 2849.
[4] T. El-Raghy, M.W. Barsoum, J. Am. Ceram. Soc. 82 (1999) 2855.
[5] M.W. Barsoum, Prog. Solid State Chem. 28 (2000) 201.
[6] M.W. Barsoum, L. Farber, T. El-Raghy, Metall. Mater. Trans. A 30 (1999) 1727.
[7] M.W. Barsoum, M. Radovic, T. Zhen, P. Finkel, S.R. Kalidindi, Phys. Rev. Lett. 94 (2005) 085501.1.
[8] T. El-Raghy, A. Zavaliangos, M.W. Barsoum, S.R. Kalidindi, J. Am. Ceram. Soc. 80 (1997) 513.
[9] A. Onodera, H. Hirano, T. Yuasa, N.F. Gao, Y. Miyamoto, Appl. Phys. Lett. 74 (1999) 3782.
[10] J.L. Jordan, T. Sekine, T. Kobayashi, X. Li, N.N. Thadhani, T. El-Raghy, M.W. Barsoum, J. Appl. Phys. 93 (2003) 9639.
[11] Z.F. Zhang, Z.M. Sun, H. Hashimoto, Metall. Mater. Trans. A 33 (2002) 3321.
[12] P. Finkel, M.W. Barsoum, T. El-Raghy, J. Appl. Phys. 87 (2000) 1701.
[13] B. Holm, R. Ahuja, B. Johansson, Appl. Phys. Lett. 79 (2001) 1450.
[14] D.A. Shockey, A.H. Marchand, S.R. Skaggs, G.E. Cort, M.W. Burkett, R. Parker, Int. J. Impact. Eng. 9 (1990) 263.
[15] D. Sherman, D.G. Brandon, J. Mater. Res. 12 (1997) 1335.
[16] D.E. Grady, J. Appl. Phys. 53 (1982) 322.
[17] C.J. Shih, M.A. Meyers, V.F. Nesterenko, S.J. Chen, Acta Mater. 48 (2000) 2399.
[18] J.Y. Wang, Y.C. Zhou, Phys. Rev. B 69 (2004) 144108–144111.
[19] Z. Rosenberg, J. Appl. Phys. 74 (1993) 752.
[20] D.E. Grady, Mech. Mater. 29 (1998) 181.
[21] I.M. Low, S.K. Lee, B.R. Lawn, J. Am. Ceram. Soc. 81 (1998) 225.
[22] L. Farber, I. Levin, M.W. Barsoum, Phil. Mag. Lett. 79 (1999) 163.
[23] B.J. Kooi, R.J. Roppen, N.J.M. Carvalho, J.Th.M. De Hosson, M.W. Barsoum, Acta Mater. 51 (2003) 2859.
[24] R. Yu, Q. Zhan, L.L. He, Y.C. Zhou, H.Q. Ye, Phil. Mag. Lett. 83 (2003) 325.